Atmos. Meas. Tech. Discuss., 5, 1515–1541, 2012
www.atmos-meas-tech-discuss.net/5/1515/2012/
doi:10.5194/amtd-5-1515-2012

Atmospheric Measurement Techniques Discussions

Characterization and airborne deployment of a new counterflow virtual impactor inlet

T. Shingler[1], S. Dey[2], A. Sorooshian[1,3], F. J. Brechtel[2], Z. Wang[1], A. Metcalf[4], M. Coggon[4], J. Mülmenstädt[5], L. M. Russell[5], H. H. Jonsson[6], and J. H. Seinfeld[4]

[1]Department of Chemical and Environmental Engineering, University of Arizona, P.O. Box 210011, Tucson, Arizona, 85721, USA
[2]Brechtel Manufacturing Inc., Hayward, California, USA
[3]Department of Atmospheric Sciences, University of Arizona, P.O. Box 210081, Tucson, Arizona, 85721, USA
[4]Departments of Environmental Science and Engineering and Chemical Engineering, California Institute of Technology, Pasadena, California, USA
[5]Scripps Institution of Oceanography, University of California, San Diego, La Jolla, California, USA
[6]Center for Interdisciplinary Remotely-Piloted Aircraft Studies, Naval Postgraduate School, Monterey, California, USA

Received: 29 January 2012 – Accepted: 5 February 2012 – Published: 14 February 2012

Correspondence to: A. Sorooshian (armin@email.arizona.edu)

Published by Copernicus Publications on behalf of the European Geosciences Union.

Abstract

A new counterflow virtual impactor (CVI) inlet is introduced with details of its design, laboratory characterization tests, and deployment on an aircraft during the 2011 Eastern Pacific Emitted Aerosol Cloud Experiment (E-PEACE). The CVI inlet addresses three key issues in previous designs; in particular, the inlet operates with: (i) negligible organic contamination; (ii) a significant sample flow rate to downstream instruments ($\sim$15 l min^{-1}) that reduces the need for dilution; and (iii) a high level of accessibility to the probe interior for cleaning. Wind tunnel experiments characterized the cut size of sampled droplets and the particle size-dependent transmission efficiency in various parts of the probe. For a range of counter-flow rates and air velocities, the measured cut size was between 8.7–13.1 µm. The percentage error between cut size measurements and predictions from aerodynamic drag theory are less than 13 %. The CVI was deployed on the Center for Interdisciplinary Remotely-Piloted Aircraft Studies (CIRPAS) Twin Otter for thirty flights during E-PEACE to study aerosol-cloud-radiation interactions off the central coast of California between July and August 2011. Results are reported to assess the performance of the inlet including comparisons of particle number concentration downstream of the CVI and cloud drop number concentration measured by two independent aircraft probes. Measurements downstream the CVI are also examined from one representative case flight coordinated with shipboard-emitted smoke that was intercepted in cloud by the Twin Otter.

1 Introduction

The aerosol nuclei that are the seeds of cloud-drops and ice are a critically important component of the atmosphere as they influence radiative transfer, visibility, and cloud formation. Characterization of the physical and chemical properties of these nuclei is needed to increase understanding of how aerosol particles affect clouds and, in turn, how clouds modify aerosol properties. Essential to understanding these interactions

AMTD
5, 1515–1541, 2012

are properties including particle size distribution, chemical composition, and hygroscopicity (Twohy et al., 1989; Hudson, 1993; Hallberg et al., 1994, 1998; Ostrom et al., 2000; Sellegri et al., 2003). Aerosol sampling from aircraft has previously relied on particle retrieval via inlets that accept all particles in the free stream, without any preferential selection for particle size. These total aerosol inlets are often unable to sufficiently decelerate the larger aerosol particles or evaporate the water residue surrounding their nuclei, typically leading to inertial deposition and droplet shatter (Huebert et al., 1990; Hudson and Frisbie, 1991; Baumgardner and Huebert, 1993; Weber et al., 1998; Hermann et al., 2001; Hegg et al., 2005). These limitations interfere with sampling a known population of aerosol in clouds, usually resulting in a mixture of interstitial aerosol particles and shattered droplets. The inlet traditionally used to sample only cloud drops is the counterflow virtual impactor (CVI), which has been discussed extensively in previous work (e.g., Ogren et al., 1985, 1987; Noone et al., 1988; Laucks and Twohy, 1998).

CVI inlets have undergone a number of design changes in the last three decades to increase their functionality and sampling efficiency. Initially, aircraft CVIs were deployed in a single fixed-tube construction, containing a large bend radius to channel the sample stream into an aircraft. Modifications to the original inlet lip structure and inner CVI geometry have led to increased collection efficiencies at lower particle diameters (Anderson et al., 1993; Schwarzenböck and Heintzenberg, 2000). Further enhancements include the addition of upstream shrouds to aid the alignment of the free stream with the inlet (Twohy, 1998). However, a number of issues still persist. For example, CVIs often are characterized by low sample flow rates and consequently need significant dilution flow so that a sufficient amount of air flow can be supplied to multiple instruments simultaneously. This is problematic for aircraft payloads containing multiple instruments downstream of the CVI that struggle with detection limit issues (e.g., Berg et al., 2009); for example, a particle-into-liquid sampler (PILS) typically requires approximately 12–15 l min^{-1} of air flow, which is a significant amount of flow when sampling downstream of a CVI (Sorooshian et al., 2006a,b; 2010). Furthermore,

AMTD
5, 1515–1541, 2012

advanced chemical composition measurement devices, such as the Aerodyne Aerosol Mass Spectrometer (AMS) are vulnerable to contamination from compounds used to fabricate older CVI designs, including siloxane sealant (Hayden et al., 2008). Finally, accessibility to the interior of older probe designs, especially for cleaning porous sections, is challenging. A number of such issues have been addressed with the development of the CVI discussed in this work.

The goal of this work is to report on a new aircraft-mountable CVI manufactured by Brechtel Manufacturing Inc. (Model 1204, www.brechtel.com). This manuscript will provide a detailed description of the inlet design, summarize laboratory characterization results from wind tunnel experiments, and relate wind tunnel results to theoretical calculations of cut size behavior using aerodynamic drag theory. Results from a recent aircraft field campaign (2011 Eastern Pacific Emitted Aerosol Cloud Experiment, E-PEACE) are presented to summarize early results and its performance, including validation of wind tunnel results for size-dependent particle transmission efficiency and droplet cut size.

2 CVI design

The theory of CVI operation is well-documented in previous work (Ogren et al., 1985, 1987; Lin and Heintzenberg, 1995). The CVI inlet in this work operates in the same manner with a detailed description of the air streams provided below and in Fig. 1. A stream of filtered and heated air (referred to as the add-flow), provided by a compressor (Gast; P/N: 75R635) and controlled by a mass-flow controller (MFC) (Alicat Scientific; P/N: MCP-50SLPM), is forced through an annular space between the exterior housing and the inner sample-stream tubing. The inner probe tube contains a porous region, 1.02 cm in length, near the tip of the inlet. The pores allow the add-flow to enter the particle stream creating a counter-flow leaving the inlet, equivalent to the difference between the add-flow and sample-flow rates. The counter-flow stream is emitted outwards from the mouth of the inlet (diameter = 2.3 mm) and creates

AMTD
5, 1515–1541, 2012

a stagnation plane immediately upstream of the inlet orifice (labeled 1 in Fig. 1). When sampling in cloud, small aerosol particles, lacking the inertia to penetrate the stagnation plane, are carried along the streamlines away from the orifice of the inlet. Particles capable of penetrating the exterior stagnation plane enter the orifice and pass into the opposing counter-flow within the inlet. The splitting of the add-flow into the counter-flow stream and sample-flow stream creates a second stagnation plane inside the probe tip (labeled 2 in Fig. 1). Any particles decelerated to a stop before reaching the second stagnation plane return back through the inlet orifice with the counter-flow. Particles and droplets that penetrate the second stagnation plane enter the CVI sample flow. The distance created between the two stagnation planes dictates the particle cut size ($D_{p,50}$), which is defined here as the size at which 50 % of the particles are sampled by the CVI, for a specific air speed and add-flow rate.

Particles that penetrate the second stagnation plane are slowed down due to expansion of the inner tube (segment C in Fig. 1), providing additional residence time to allow water associated with particles to evaporate in the heated sample-flow stream. The sample-flow stream is directed to a 90° bend in the tubing and into the aircraft. Very large droplets (>40 µm diameter) with a sufficiently high amount of inertia and long evaporation times cannot make the turn and impact in an extended region, referred to as the particle trap (segment E in Fig. 1). The CVI in this study was optimized for 15 l min^{-1} of sample air flow to accommodate the increased flow rate requirements to operate multiple instruments downstream of the inlet at the same time; as noted earlier, a limitation in previous designs was the large amount of dilution flow that needed to be added to the sample flow to provide enough sample flow to instruments. The sample stream flow rate is kept at a constant 15 l min^{-1} by a MFC (Alicat Scientific; P/N: MCP-50SLPM).

To address the issue of organic contamination, the inlet is constructed such that all surfaces that contact the counter-flow and sample air flow are either stainless steel or aluminum. It is further noted that the tubing in Segment B of Fig. 1 is interchangeable to allow more flexibility in optimizing for different inlet cut sizes and for cleaning purposes.

AMTD
5, 1515–1541, 2012

3 Laboratory characterization

CVI characterization experiments were performed using the BMI wind tunnel following methods described in Anderson et al. (1993). A dispersion of hollow glass spheres (Particle diameter, D_p, range = 2–20 µm, mean diameter = 8 µm, $\rho = 1.1\,\mathrm{g\,cm^{-3}}$, Polysciences, P/N: 19823) was introduced to the wind tunnel. A TSI Model 3321 Aerodynamic Particle Sizer (APS) obtained number-size distributions sampled by the CVI inlet. Figure 2 depicts the wind tunnel sampling configuration.

The glass sphere distribution introduced into the wind tunnel was sampled by the CVI operating in one of two modes: isokinetic sampling or CVI sampling. Total sample-flow drawn by the inlet was kept constant at $15\,\mathrm{l\,min^{-1}}$ for each sampling mode. Isokinetic sampling was performed by drawing only $15\,\mathrm{l\,min^{-1}}$ of sample flow through the inlet orifice with no add-flow, and setting the wind tunnel velocity sufficiently low to create isokinetic sampling conditions at the CVI tip. For operation in CVI sampling mode, the add-flow is supplied and the wind tunnel is run at the full desired velocity. For the characterization experiments the tunnel was operated at two velocities: $50\,\mathrm{m\,s^{-1}}$ and $100\,\mathrm{m\,s^{-1}}$, where the former is similar to the air speed of the aircraft during E-PEACE. The add-flow rate was varied over the 16–23 $\mathrm{l\,min^{-1}}$ range to characterize a range of cut sizes. A total of 24 trials were performed for each of the following seven conditions (see also Table 1): isokinetic sampling mode and CVI sampling mode with add-flow rates of 16, 19, and 23 $\mathrm{l\,min^{-1}}$ and air speeds of 50 and $100\,\mathrm{m\,s^{-1}}$. Resultant counterflow rates were 1, 4, and 8 $\mathrm{l\,min^{-1}}$, respectively.

Experimental cut size in the wind tunnel was determined by taking the ratio of the sampled CVI number-size distribution to the sampled isokinetic number-size distribution. Sampling in isokinetic mode provides a reference number-size distribution of the glass beads, to which the distribution obtained from CVI sampling mode can be compared. As described in Anderson et al. (1993), a normalization scheme where each APS size bin is divided by the sum of counts in the bins between 17–20 µm was applied

AMTD
5, 1515–1541, 2012

prior to calculating the ratio of the measured CVI number-size distribution to reference isokinetic distribution.

Experimentally determined cut sizes are summarized in Fig. 3 and Table 1. As expected, the cut size grew with increasing add-flow rate and decreasing wind tunnel air velocity. The cut size that corresponds to the conditions in E-PEACE (air speed = 50 m s^{-1}, add-flow rate = 16 l min^{-1}) is 11 µm. The overall range of cut sizes identified in the experiments for the range of flow conditions was 8.7–13.1 µm. Previous work has defined cut sharpness as $\sigma = (D_{p,84}/D_{p,16})^{1/2}$, with values ranging between 1.08–1.13 for at least one other CVI design (Anderson et al., 1993). Here we define cut sharpness as $\sigma = (D_{p,69}/D_{p,31})^{1/2}$ to stay consistent with the range of transmission efficiencies obtained in the experiments. Table 1 shows that the modified cut sharpness values range from 1.15–1.22 for the 50 m s^{-1} air speed condition and 1.28–1.34 for 100 m s^{-1}.

It is useful to compare the cut sizes predicted by aerodynamic drag theory to the experimentally determined values obtained in the wind tunnel experiments, as demonstrated in previous studies (e.g., Noone et al., 1988; Anderson et al., 1993). Here we adopt most of the notation and the numerical integration technique summarized by Anderson et al. (1993), where the size-dependent impaction distance is estimated between the stagnation planes using the position-dependent counter-flow gas velocity in the counter-flow region. The numerical integration is performed assuming the particle impaction starts at a distance, L_{cur}, away from the probe tip. The change in particle velocity is calculated along the path of impaction up to the internal stagnation plane. Particles which maintain a positive velocity through the internal stagnation plane are collected by the inlet. The theoretical cut size, $D_{p,50}$, is determined by finding the particle diameter required to have a stopping distance equal to the length of the impaction path, L_{CVI}. The distance L_{CVI} is defined in Eq. (1), where L_{min} is the fixed distance from the probe tip to the start of the porous tube and L_{por} is the length from the start of the porous tube to the internal stagnation plane:

$$L_{CVI} = L_{cur} + L_{min} + L_{por}. \quad (1)$$

AMTD
5, 1515–1541, 2012

Variances between predicted and measured cut sizes are accounted for by adjusting the impaction starting point, L_{cur}. Previous cut size prediction methods have defined L_{cur} as a constant ($g(r)$ or C_1) multiplied by the outer probe radius, used to account for streamline curvature of air near the orifice of the probe (Noone et al., 1988; Anderson et al., 1993). Data obtained during the wind tunnel experiments were used to predict an average C_1 value of 1.25 over the range of counter-flow rates from 1–8 l min^{-1} and air speeds from 50–100 m s^{-1}. With this C_1 value, the error between the predicted and measured cut sizes is less than 12.6 % for the six conditions tested in Table 1.

Characterization in the wind tunnel also included evaluating particle size-dependent losses in the CVI body, mainly as a result of inertial deposition. Losses were evaluated by comparing size distributions obtained while sampling through different portions of the sampling train to the distribution of glass beads measured by the APS with no CVI tip assembly installed in the wind tunnel. Experiments were performed to isolate losses for separate segments of the wind tunnel sampling train. Particle transmission was measured through a long sampling tube labeled 3 in Fig. 2, followed by examining losses through the sample expansion section coupled to the long sampling tube (segments 2 and 3 in Fig. 2). Finally, a comparison was made to a sample from the combined segments (segments 1, 2, and 3 in Fig. 2). From this, losses in segments 1 and 2 (Fig. 2) individually were determined. It should be noted that the wind tunnel sampling configuration differs from the configuration of the inlet as installed on an aircraft. Only losses in segments 1 and 2, which correspond to segments B and C (Fig. 1), are relevant to the aircraft installation. These losses are presented in Fig. 4, showing each segment's individual contribution and the combined effect. Tubing prior to the expansion is shown to be a larger source for particle losses via turbulent deposition as compared to the expansion. At the expected cut size of 11 µm during E-PEACE the total losses amount to approximately 57 % and increase to 72 % at a particle diameter of 20 µm. It is noted that the tubing prior to the expansion is interchangeable, and losses can be significantly reduced by using a shortened tube. Ongoing work is addressing these losses. However, the results in Fig. 4 are critical for interpreting the

AMTD
5, 1515–1541, 2012

E-PEACE field data, especially for validating the cut size measurements from the wind tunnel testing.

4 Field deployment and first results

The CVI was deployed on the Center for Interdisciplinary Remotely-Piloted Aircraft Studies (CIRPAS) Twin Otter during the 2011 E-PEACE field study off the central coast of California. E-PEACE consisted of 30 research flights to study aerosol-radiation-cloud-precipitation interactions over the Eastern Pacific Ocean during the summertime when stratocumulus cloud decks are persistent. The domain of the flights ranged between 34° N–40° N and 121.5° W–125° W. Nine of the Twin Otter flights were coordinated with the Research Vessel *Point Sur*, which generated smoke each of these days to allow the aircraft to study the effects of a known source of aerosol on cloud microphysical and macrophysical properties. A comprehensive description of this field study is forthcoming.

Six different instruments conducted measurements downstream of the CVI in stratocumulus clouds during E-PEACE (Fig. 5). A three-way valve was used to cycle these six instruments between the CVI in cloud and a sub-isokinetic aerosol inlet out of cloud. When sampling was conducted through the CVI in cloud, the total flow required by the instruments was 4.2 l min^{-1} with the CVI sample-flow MFC controlling the remaining 10.8 l min^{-1}. When the instruments downstream of the CVI were not sampling from the CVI sample-flow stream, the MFC allowed the full 15 l min^{-1} through the sample stream. The instruments included a condensation particle counter (CPC; TSI Model 3010) to quantify total aerosol concentration (N_a). Aerosol size distribution data were obtained by a cylindrical scanning differential mobility analyzer (DMA; TSI Model 3081) coupled to a condensation particle counter (CPC; TSI Model 3010). Aerosol particles were dried prior to entering the DMA for sizing. Aerosol absorption and scattering coefficients were measured using a three-wavelength Photoacoustic Soot Spectrometer (PASS-3; Droplet Measurement Technologies). A continuous flow thermal gradient

AMTD
5, 1515–1541, 2012

cloud condensation nuclei counter (CCNc, Droplet Measurement Technologies Inc.; Roberts and Nenes, 2005) was used to quantify the number of particles that activated at supersaturations ranging from 0.2 % to 0.8 %. Black carbon (BC) mass measurements were obtained using a single particle soot photometer instrument (SP2; Droplet Measurement Technologies) (Schwarz et al., 2006; Metcalf et al., 2012). Measurements of inorganic mass (sulfate, nitrate, ammonium) and total non-refractory organic mass were obtained with a compact Time of Flight Aerosol Mass Spectrometer (Aerodyne C-ToF-AMS) (Drewnick et al., 2005). A comprehensive analysis of the detailed measurements of droplet residual particle properties will be addressed in a subsequent study.

Critical to the examination of field data is the quantification of the "enhancement factor" as a result of the ambient aerosol concentration being concentrated in the CVI inlet according to the following equation:

$$\mathrm{EF} = \frac{A_{\mathrm{tip}} V_{\mathrm{plane}}}{q_{\mathrm{sample}}} \tag{2}$$

where: EF is the enhancement factor, A_{tip} is the area of the inlet tip where drops enter, V_{plane} is aircraft velocity, and q_{sample} is the volumetric flow rate of sampled air in the CVI inlet. A_{tip} is 1.67×10^{-5} m^2, q_{sample} is 15 l min^{-1}, and the aircraft velocity was usually near 50 m s^{-1}. The latter air velocity, which was tested in the wind tunnel experiments, coincides with an EF of 3.28.

It is possible for small amounts of particles with sizes below the $D_{\mathrm{p,50}}$ to undergo "breakthrough" by way of collisions with larger particles, or wake capture (Pekour and Cziczo, 2011). To identify whether there was any breakthrough of small particles through the CVI, the inlet was operated for small periods of time during some flights in clear air just as it would be in cloud. To ensure the aircraft was in clear air for this analysis, data were used when the cloud liquid water content (LWC), measured by a PVM-100 probe (Gerber et al., 1994), was less than 0.01 g m^{-3}. When applying an add-flow ranging between 16–19 l min^{-1}, the CPC concentration in clear

AMTD
5, 1515–1541, 2012

air (LWC = 0.002 ± 0.009 g m^{-3}) was 0.08 ± 0.09 cm^{-3}. The ratio of the CPC concentration downstream of the CVI relative to an identical instrument sampling simultaneously downstream of a sub-isokinetic inlet was 0.0001 ± 0.0002, indicating that particle breakthrough and any type of small particle contamination were absent.

Prior to E-PEACE, test flights were conducted to determine the flow angle at the location of the CVI intake. The location was only a short distance forward of the port wing root. Significant angles between the oncoming air flow and the CVI inlet will increase the likelihood of droplet impaction and shatter on inlet surfaces. A Rosemount 858 flow angle probe indicated a 10° up-wash at that location during flight, and flow visualization using yarn taped to the probe's tip verified this angle. To minimize the chance of flow separation in the sampling inlet, and possible particle losses, the CVI probe was angled into the flow and mounted on the airplane with a 10° downward tilt.

Critical to the characterization of the field performance of the CVI is the comparison of particle number concentration (N_a) measured by the CPC downstream of the CVI to in-situ measurements of cloud drop concentration (N_d). For the latter measurement, data were obtained using a Cloud and Aerosol Spectrometer (CAS; $D_p \sim 1$–55 µm; Droplet Measurement Technologies, Inc.; Baumgardner et al., 2001) and a Cloud Droplet Probe (CDP; $D_p \sim 1$–51 µm; Droplet Measurement Technologies, Inc.; Lance et al., 2010). CVI data are presented for the first 11 flights (8 July–23 July) since both cloud probes were operational during this time range. The comparison involved applying the EF to the CPC data and the size-dependent transmission efficiency results in Fig. 4 to the cloud probe data to assess the level of agreement between N_a and N_d. Figure 6 summarizes the comparison of N_a to N_d, where the latter was quantified using a variety of minimum drop sizes smaller and larger than the cut size identified from the wind tunnel experiments. It is noted that the CAS instrument has larger bin widths (i.e. bin boundaries of 9.39, 12.52, and 16.28 µm) around the vicinity of the wind tunnel CVI cut size (11 µm) relative to the CDP (i.e. bin boundaries of 10.37, 11.35, 12.4 µm). The analysis was conducted for the following conditions: (i) LWC greater than 0.05 g m^{-3} to ensure the aircraft was in cloud; (ii) aircraft speeds between 45–60 m s^{-1} to allow

AMTD
5, 1515–1541, 2012

for a meaningful comparison with the wind tunnel results at 50 m s^{-1}; (iii) the add-flow rate was either 16 or 17 l min^{-1}. The agreement between N_a and N_d is best when the CAS drop distributions were integrated above 12.52 µm ($r^2 = 0.71$) and when the CDP distributions were integrated above 10.37 µm ($r^2 = 0.84$). The slope of N_a to N_d plots were closest to unity (0.90–0.97) for these two conditions with decreasing values when integrating the cloud drop distribution above larger sizes, indicating that the CVI cut size was close to 11 µm.

One case flight is examined in greater detail to examine the temporal trends in N_a and N_d in cloud. The focus of this analysis is Research Flight 6 on 16 July 2011, which was a flight coordinated between the Twin Otter and the Research Vessel *Point Sur*. The latter was generating smoke with an on-board smoke generator, and the aircraft probed the properties of the smoke both below cloud and in cloud. The flight tracks of the Twin Otter are shown in Fig. 7 superimposed on GOES-11 visible satellite imagery to show the structure of the clouds during the period of the flight. The aircraft conducted detailed measurements of aerosol properties below the cloud deck, within the cloud at different altitudes, and above the cloud deck. Figure 8 shows a representative 20 min flight leg when the Twin Otter was sampling in cloud, during which time the aircraft sampled the ship smoke in cloud numerous times. Based on a threshold LWC value of 0.05 g m^{-3}, this particular cloud deck had a base and top of approximately 70 m and 200 m, respectively. During the flight leg shown, the aircraft ascended from a region slightly above the bases to near the middle of the cloud deck, which is reflected in the increase in droplet size (Fig. 8; bottom panel). The N_a measurement downstream of the CVI is shown to exhibit the same temporal behavior as N_d measured by the CAS and CDP, when the size distributions of the two latter cloud probes were integrated at or below the expected cut size of the CVI (~11 µm). When the aircraft flew in cloud regions influenced by the ship smoke, both N_a and N_d levels are enhanced with a reduction in drop size, which is consistent with the Twomey Effect (Twomey, 1974).

AMTD
5, 1515–1541, 2012

There was no indication of organic contamination from the inlet during E-PEACE. AMS measurements of non-refractory organics in droplet residual particles during clean marine background conditions were typically below the AMS organic detection limit of 0.1 $\mu g\,m^{-3}$. Increases in the AMS organic mass concentration corresponded with enhancements in other measurements indicating signs of increasing pollution (e.g., CPC, CDP, CAS, and other aerosol/cloud instruments); therefore, E-PEACE CVI measurements indicate that organic signals are a measurement of cloud nuclei chemistry and are uninfluenced by artifacts associated with the inlet material of construction.

An example of aerosol composition measurements downstream of the CVI is shown in Fig. 9. Four representative AMS mass fraction pie charts are shown to represent the following from Flight 6: background marine aerosol below cloud; background in cloud (CVI); *Point Sur* ship smoke below cloud; and *Point Sur* ship smoke in cloud (CVI). Only sulfate and organic contributions are shown since the other non-refractory constituents (i.e., ammonium, chloride, nitrate) were below detection limits. Organics were the dominant non-refractory component of the sub-micrometer aerosol, and this is especially the case for the *Point Sur* smoke, which was nearly entirely organic (~99 %) when sampled below cloud during this flight. The droplet residual samples examined during the time when the *Point Sur* smoke was intercepted in cloud were mainly of organic nature (~ 92%), as compared to the background cloud conditions (~ 67%).

Figure 9 also shows log-normal fits to the mean size distributions obtained from a scanning differential mobility analyzer during the same time periods as the AMS pie charts. The background aerosol below cloud, sampled from the sub-isokinetic inlet, was fit to a two lognormal mode function; the size distributions behind the CVI were fit to a single-term log-normal function. The *Point Sur* smoke crossings below cloud were sufficiently narrow that an entire DMA scan (~110 s) did not properly capture the size distribution of this source, and thus only one average distribution is presented. The background sub-cloud size distribution exhibits a bimodal character with a sub-100 nm mode and a larger mode indicative of cloud-processed aerosol. The droplet residual particle size distributions were unimodal with the modal diameter at approximately

AMTD
5, 1515–1541, 2012

200 nm, indicating that the larger of the two modes below cloud was most effective at activating into droplets. More detailed results of the physicochemical properties of droplet residual particles from the E-PEACE study will be forthcoming,

5 Conclusions

A new CVI inlet has been characterized using wind tunnel experiments and deployed on the CIRPAS Twin Otter for 30 flights during the 2011 E-PEACE field campaign. With straightforward modifications, the inlet can also be deployed at ground or mountaintop sites to sample fog and orographic clouds. With a fixed sample flow rate of 15 l min^{-1}, the wind tunnel experiments explored a range of add-flow rates (16–23 l min^{-1}) and air velocities (50–100 m s^{-1}) to obtain inlet cut sizes between 8.7–13.1 µm. Calculated cut sizes from aerodynamic drag theory agree with measured values to within 13 %. When applying size-dependent transmission efficiency results from the wind tunnel to aircraft data, there was good agreement between particle concentration (N_a) measurements downstream of the CVI and cloud drop concentrations (N_d) measured by two independent cloud probes. When integrating the drop size distributions above a diameter close to the expected 11 µm cut size (based on wind tunnel testing), slopes from N_d–N_a plots were 0.90–0.97 and correlation coefficients (r^2) were 0.71–0.84. Representative data from a case study flight show excellent temporal agreement between N_a and N_d, especially when a smoke plume from a ship was intercepted in cloud. This resulted in sudden enhancements in drop concentration and reductions in drop size. Size distribution measurements of droplet residual particles during this flight show that the modal diameter of particles activated into drops was approximately 200 nm both in and out of the smoke. Aerosol composition measurements from an AMS indicate that the majority of the sub-micrometer non-refractory mass was from organic species, with the remaining constituent being sulfate. No indication of organic contamination from the inlet itself was found. Furthermore, no evidence of particle breakthrough or small particle contamination was observed during CVI sampling during E-PEACE.

AMTD
5, 1515–1541, 2012

Acknowledgements. This work was funded by an ONR DURIP grant (N00014-11-1-0783), an ONR YIP award (N00014-04-1-0018), ONR grant N00014-10-1-0200, NSF grants AGS-1008848 and AGS1013423, and Sea Spray Research, Inc. The authors gratefully acknowledge the crew of both the CIRPAS Twin Otter and the Research Vessel *Point Sur*.

References

Anderson, T. L., Charlson, R. J., and Covert, D. S.: Calibration of a counterflow virtual impactor at aerodynamic diameters from 1 to 15 µm, Aerosol Sci. Tech., 19, 17–329, 1993.

Baumgardner, D. and Huebert, B.: The Airborne Aerosol Inlet Workshop – meeting report, J. Aerosol Sci., 24, 835–846, 1993.

Baumgardner, D., Jonsson, H., Dawson, W., O'Connor, D., and Newton, R.: The cloud, aerosol and precipitation spectrometer: a new instrument for cloud investigations, Atmos. Res., 59–60, 251–264, 2001.

Berg, L. K., Berkowitz, C. M., Ogren, J. A., Hostetler, C. A., Ferrare, R. A., Dubey, M. K., Andrews, E., Coulter, R. L., Hair, J. W., Hubbe, J. M., Lee, Y. N., Mazzoleni, C., Olfert, J., and Springston, S. R.: Overview of the Cumulus Humilis Aerosol Processing Study, B. Am. Meteorol. Soc., 90, 1653–1667, 2009.

Drewnick, F., Hings, S. S., DeCarlo, P., Jayne, J. T., Gonin, M., Fuhrer, K., Weimer, S., Jimenez, J. L., Demerjian, K. L., Borrmann, S., and Worsnop, D. R.: A new time-of-flight aerosol mass spectrometer (TOF-AMS) – instrument description and first field deployment, Aerosol Sci. Tech., 39, 637–658, 2005.

Gerber, H., Arends, B. G., and Ackerman, A. S.: New microphysics sensor for aircraft use, Atmos. Res., 31, 235–252, 1994.

Hallberg, A., Noone, K. J., Ogren, J. A., Svenningsson, I. B., Flossmann, A., Wiedensohler, A., Hansson, H. C., Heintzenberg, J., Anderson, T. L., Arends, B. G., and Maser, R.: Phase partitioning of aerosol particles in clouds at Kleiner Feldberg, J. Atmos. Chem., 19, 107–127, 1994.

Hallberg, A., Noone, K. J., and Ogren, J. A.: Aerosol particles and clouds: which particles form cloud-droplets?, Tellus B, 50, 59–75, 1998.

Hayden, K. L., Macdonald, A. M., Gong, W., Toom-Sauntry, D., Anlauf, K. G., Leithead, A.,

AMTD

5, 1515–1541, 2012

Li, S.-M., Leaitch, W. R., and Noone, K.: Cloud processing of nitrate, J. Geophys. Res., 113, D18201, doi:10.1029/2007JD009732, 2008.
Hegg, D. A., Covert, D. S., Jonsson, H., and Covert, P. A.: Determination of the transmission efficiency of an aircraft aerosol inlet, Aerosol Sci. Tech., 39, 966–971, 2005.
Hermann, M., Stratmann, F., Wilck, M., and Wiedensohler, A.: Sampling characteristics of an aircraft-borne aerosol inlet system, J. Atmos. Ocean Tech., 18, 7–19, 2001.
Hudson, J. G.: Cloud condensation nuclei near marine cumulus, J. Geophys. Res., 98, 2693–2702, 1993.
Hudson, J. G. and Frisbie, P. R.: Cloud condensation nuclei near marine stratus, J. Geophys. Res., 96, 20795–20808, 1991.
Huebert, B. J., Lee, G., and Warren, W. L.: Airborne aerosol inlet passing efficiency measurement, J. Geophys. Res., 95, 16369–16381, 1990.
Lance, S., Brock, C. A., Rogers, D., and Gordon, J. A.: Water droplet calibration of the Cloud Droplet Probe (CDP) and in-flight performance in liquid, ice and mixed-phase clouds during ARCPAC, Atmos. Meas. Tech., 3, 1683–1706, doi:10.5194/amt-3-1683-2010, 2010.
Laucks, M. L. and Twohy, C. H.: Size-dependent collection efficiency of an airborne counterflow virtual impactor, Aerosol Sci. Tech., 28, 40–61, 1998.
Lin, H. and Heintzenberg, J.: A theoretical-study of the counterflow virtual impactor, J. Aerosol Sci., 26, 903–914, 1995.
Noone, K. J., Ogren, J. A., Heintzenberg, J., Charlson, R. J., and Covert, D. S.: Design and calibration of a counterflow virtual impactor for sampling of atmospheric fog and cloud-droplets, Aerosol Sci. Tech., 8, 235–244, 1988.
Ogren, J. A., Heintzenberg, J., and Charlson, R. J.: In-situ sampling of clouds with a droplet to aerosol converter, Geophys. Res. Lett., 12, 121–124, 1985.
Ogren, J. A., Heintzenberg, J., and Charlson, R. J.: Virtual impactor, U.S. Patent No. 4,689,052, 1987.
Ostrom, E., Noone, K. J., and Pockalny, R. A.: Cloud-droplet residual particle microphysics in marine stratocumulus clouds observed during the Monterey Area Ship Track experiment, J. Atmos. Sci., 7, 2671–2683, 2000.
Pekour, M. S. and Cziczo, D. J.: Wake capture, particle breakup, and other artifacts associated with counterflow virtual impaction, Aerosol Sci. Tech., 45, 758–764, 2011.
Roberts, G. C. and Nenes, A.: A continuous-flow streamwise thermal-gradient CCN chamber for atmospheric measurements, Aerosol Sci. Tech., 39, 206–221,

AMTD
5, 1515–1541, 2012

doi:10.1080/027868290913988, 2005.
Schwarz, J. P., Gao, R. S., Fahey, D. W., Thomson, D. S., Watts, L. A., Wilson, J. C., Reeves, J. M., Darbeheshti, M., Baumgardner, D. G., Kok, G. L., Chung, S. H. Schulz, M., Hendricks, J., Lauer, A., Karcher, B., Slowik, J. G., Rosenlof, K. H., Thompson, T. L., Langford, A. O., Loewenstein, M., and Aikin, K. C.: Single-particle measurements of midlatitude black carbon and light-scattering aerosols from the boundary layer to the lower stratosphere, J. Geophys. Res., 111, D16207, doi:10.1029/2006JD007076, 2006.
Schwarzenböck, A. and Heintzenberg, J.: Cut size minimization and cloud element break-up in a ground-based CVI, J. Aerosol Sci., 31, 477–489, 2000.
Sellegri, K., Laj, P., Dupuy, R., Legrand, M., Preunkert, S., and Putaud, J. P.: Size-dependent scavenging efficiencies of multicomponent atmospheric aerosols in clouds, J. Geophys. Res., 108, 4334, doi:10.1029/2002JD002749, 2003.
Sorooshian, A., Brechtel, F. J., Ma, Y. L., Weber, R. J., Corless, A., Flagan, R. C., and Seinfeld, J. H.: Modeling and characterization of a particle-into-liquid sampler (PILS), Aerosol Sci. Tech., 40, 396–409, doi:10.1080/02786820600632282, 2006a.
Sorooshian, A., Varutbangkul, V., Brechtel, F. J., Ervens, B., Feingold, G., Bahreini, R., Murphy, S. M., Holloway, J. S., Atlas, E. L., Buzorius, G., Jonsson, H., Flagan, R. C., and Seinfeld, J. H.: Oxalic acid in clear and cloudy atmospheres: analysis of data from International Consortium for Atmospheric Research on Transport and Transformation 2004, J. Geophys. Res., 111, D23S45, doi:10.1029/2005JD006880, 2006b.
Sorooshian, A., Murphy, S. M., Hersey, S., Bahreini, R., Jonsson, H., Flagan, R. C., and Seinfeld, J. H.: Constraining the contribution of organic acids and AMS *m/z* 44 to the organic aerosol budget: on the importance of meteorology, aerosol hygroscopicity, and region, Geophys. Res. Lett., 37, L21807, doi:10.1029/2010GL044951, 2010.
Twohy, C. H.: Model calculations and wind tunnel testing of an isokinetic shroud for high-speed sampling, Aerosol Sci. Tech., 29, 261–280, 1998.
Twohy, C. H., Clarke, A. D., Warrcn, S. G., Radke, L. F., and Charlson, R. J.: Light absorbing material extracted from cloud-droplets and its effect on cloud albedo, J. Geophys. Res., 94, 8623–8631, 1989.
Twomey, S.: Pollution and planetary albedo, Atmos. Environ., 8, 1251–1256, 1974.
Weber, R. J., Clarke, A. D., Litchy, M., Li, J., Kok, G., Schillawski, R. D., and McMurry, P. H.: Spurious aerosol measurements when sampling from aircraft in the vicinity of clouds, J. Geophys. Res., 103, 28337–28346, 1998.

AMTD
5, 1515–1541, 2012

Table 1. Cut size behavior of the CVI inlet at different simulated air velocities and add-flow rates. Results are shown for wind tunnel experiments and theoretical calculations based on a numerical integration technique described by Anderson et al. (1993) using a C_1 value of 1.25. Values in parentheses in the "Measured" columns correspond to the cut sharpness defined as $(D_{p,69}/D_{p,31})^{1/2}$. Values in parentheses in the "Predicted" columns signify the percent error between measured and predicted values.

	Measured		Predicted	
Add-flow ($l\,min^{-1}$)	$D_{p,50}$ at 50 $m\,s^{-1}$ (μm)	$D_{p,50}$ at 100 $m\,s^{-1}$ (μm)	$D_{p,50}$ at 50 $m\,s^{-1}$ (μm)	$D_{p,50}$ at 100 $m\,s^{-1}$ (μm)
16	11.0 (1.22)	8.7 (1.34)	10.8 (1.8 %)	7.6 (12.6 %)
19	12.5 (1.20)	9.8 (1.28)	12.9 (3.2 %)	8.9 (9.2 %)
23	13.1 (1.15)	10.2 (1.30)	14.7 (12.2 %)	10.0 (2.0 %)

AMTD
5, 1515–1541, 2012

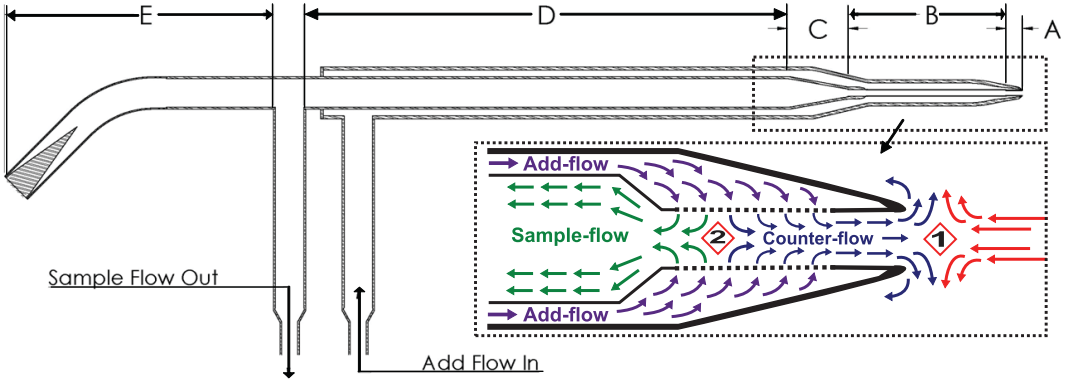

Fig. 1. Schematic depiction of the BMI CVI and flows innate to its operation. Sampled air enters the CVI through the inlet nozzle and passes through a region containing a porous tube where the heated counter-flow is introduced (A). The resulting sample flow enters an extension tube (B), before the expansion region (C). The particles then travel through additional plumbing (D) and enter the aircraft body for sample feed to instruments. Entities too large to bend into the aircraft are collected in a particle trap (E). Two stagnation planes (labeled 1 and 2) are generated between opposing flow directions. The cut size is governed by the velocity of the ambient air flow and the distance between the two stagnation planes.

AMTD
5, 1515–1541, 2012

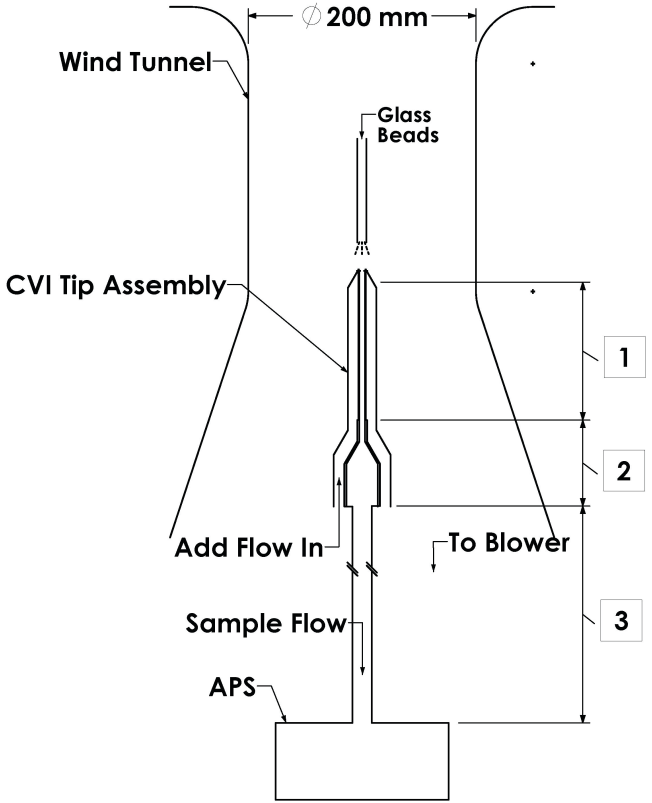

Fig. 2. Schematic of BMI wind tunnel set-up. A dispersion of glass sphere beads is introduced to the wind tunnel and the inlet operates in either isokinetic or CVI sampling mode. The ratio of the number size distributions measured by an aerodynamic particle sizer (APS) is used to determine the transmission efficiency of the inlet. These experiments followed the methods summarized by Anderson et al. (1993). The number labels are used to distinguish between different sections of the sampling train.

AMTD
5, 1515–1541, 2012

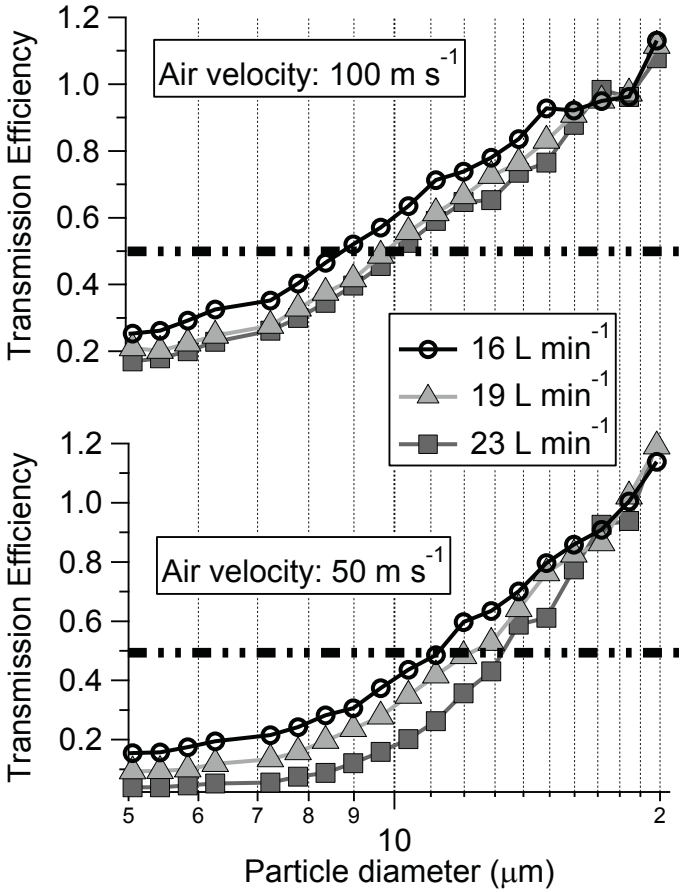

Fig. 3. Transmission efficiency of hollow glass beads at different add-flow rates based on experiments conducted with the BMI wind tunnel at different air velocity conditions (50 and 100 m s^{-1}). The dashed horizontal lines correspond to 50 % transmission efficiency, which defines the inlet cut size ($D_{p,50}$).

AMTD
5, 1515–1541, 2012

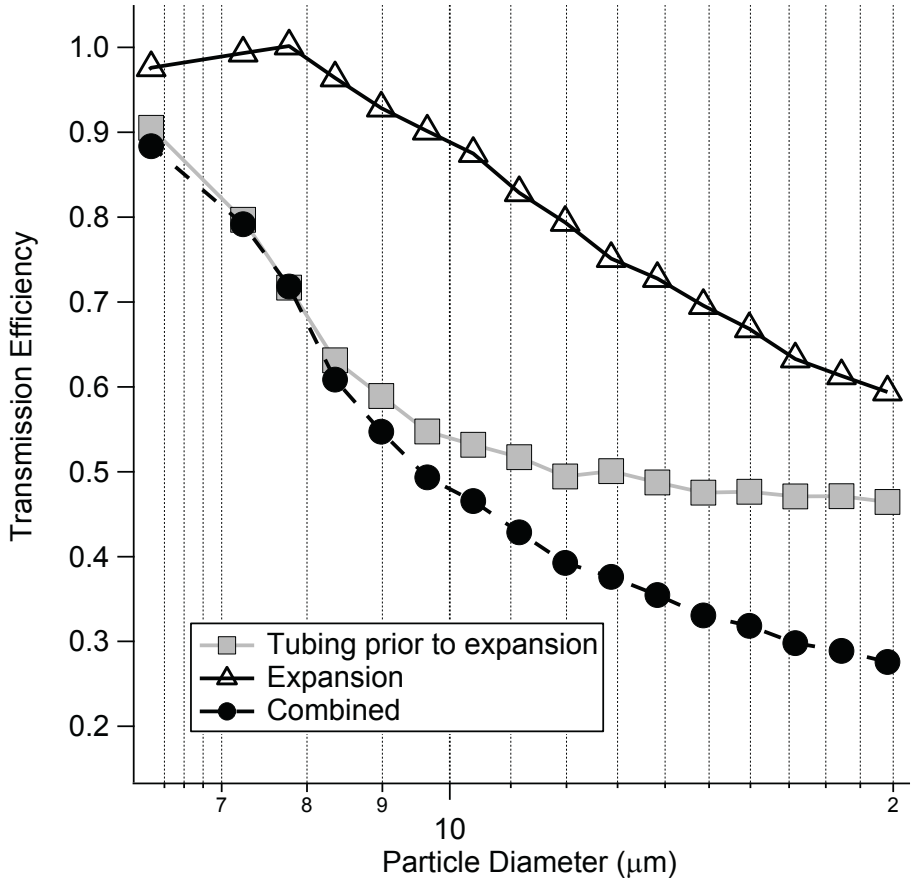

Fig. 4. Transmission efficiency for hollow glass beads in various parts of the CVI inlet based on wind tunnel experiments. "Tubing prior to expansion" refers to segment (B) in Fig. 1 and "Expansion" refers to segment (C) in Fig. 1.

AMTD
5, 1515–1541, 2012

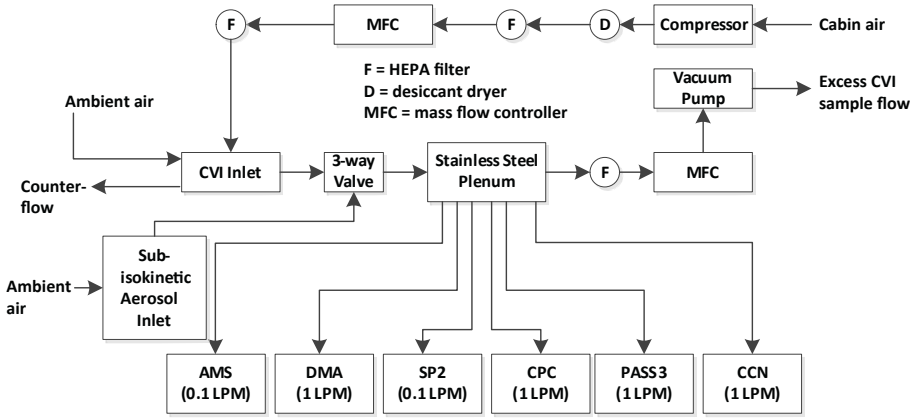

Fig. 5. Schematic of the sample air flow path through both the sub-isokinetic aerosol inlet (clear air sampling) and the CVI (in-cloud sampling) on the CIRPAS Twin Otter during the 2011 E-PEACE experiment. Six instruments characterized aerosol physicochemical properties downstream of the CVI inlet with their respective flow rates shown (total = 4.2 l min^{-1}). As the total sample flow rate provided was 15 l min^{-1}, the excess sample flow (10.8 l min^{-1}) was diverted out of the aircraft by a vacuum pump.

AMTD
5, 1515–1541, 2012

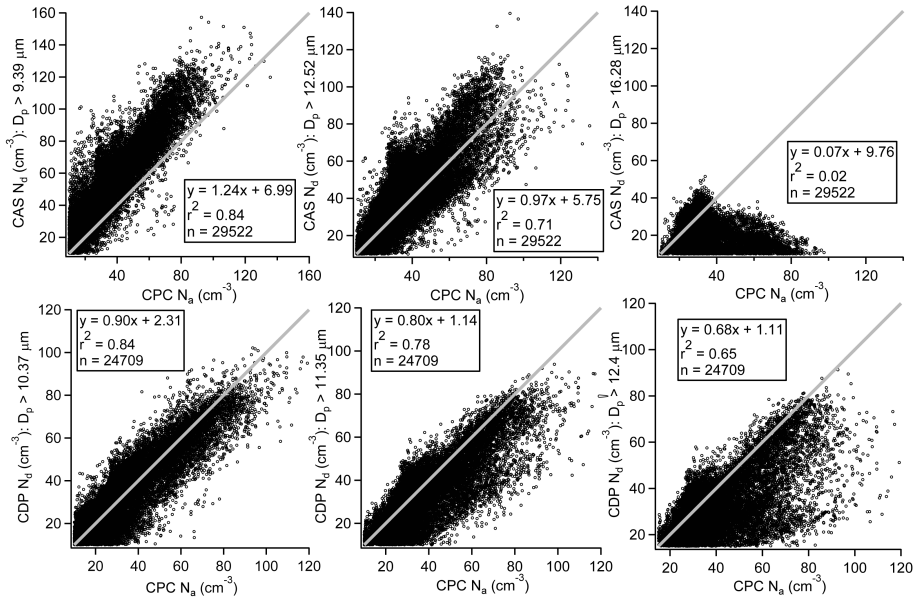

Fig. 6. Comparison of corrected total particle concentration (N_a) measured behind the CVI by a CPC and total cloud drop concentration (N_d) measured by two independent cloud probes (CDP and CAS). For both cloud probes, N_d is reported above three different minimum drop sizes around the expected cut size (~11 µm) of the CVI at 50 m s^{-1} for the usual add-flow rate applied (~16 l min^{-1}) based on wind tunnel results. Data are shown when the in-cloud liquid water content exceeded 0.05 g m^{-3}, when the aircraft speed was between 45–60 m s^{-1}, and when the add-flow rate was between 16–17 l min^{-1}. The gray shaded lines signify the 1-to-1 line. The reason the slope of the top right panel is much lower than the rest is that the majority of the sampled cloud drop number concentrations were typically at lower diameters.

AMTD
5, 1515–1541, 2012

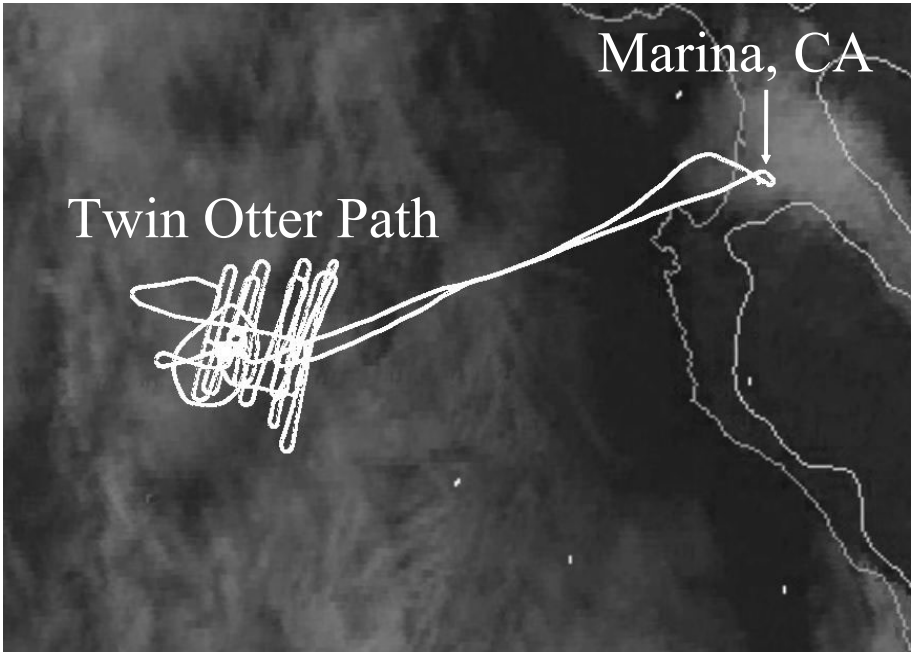

Fig. 7. GOES-11 visible satellite imagery at 18:00 UTC on 16 July 2011 with the superposition of the CIRPAS Twin Otter, which was based in Marina, California. The high density of flight track points to the far west coincides with when the aircraft was probing the smoke plume generated by the *Point Sur* ship. The corresponding time series of aircraft data is shown in Fig. 8 with aerosol size distribution and composition data shown in Fig. 9.

AMTD
5, 1515–1541, 2012

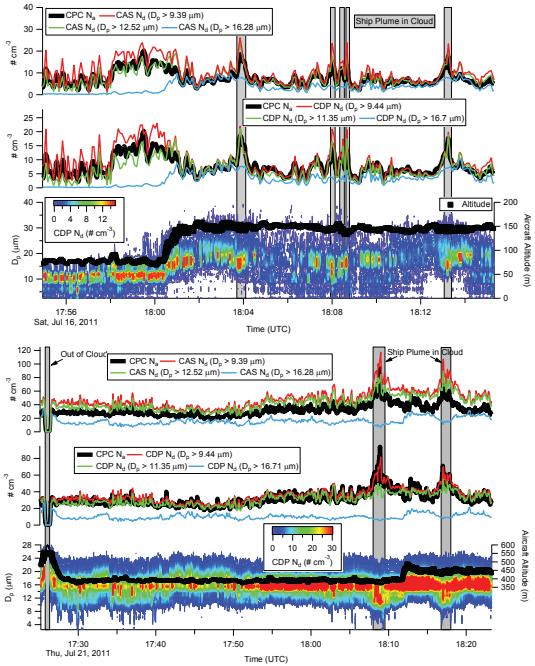

Fig. 8. Time series of aircraft data collected during Flight 6 of the 2011 E-PEACE campaign on 16 July 2011. The 20-min time segment coincides with when the Twin Otter was flying in a stratocumulus cloud deck of the coast of Monterey, California. This flight was coordinated with the Research Vessel *Point Sur*, which generated smoke that influenced the cloud in the several gray shaded regions of the time series via enhancements in drop concentration and reductions in drop size. The total particle concentration (N_a) measured behind the CVI by a CPC (with enhancement factor, ~3.3, applied) is compared to total cloud drop concentration (N_d) measured by two independent probes, where N_d is integrated above three different diameters to further constrain the CVI cut size diameter. Size-dependent transmission efficiency losses from Fig. 4 are applied to the N_d data. The aircraft altitude marker size is proportional to LWC (range ~0.05–0.30 g m^{-3}).

AMTD
5, 1515–1541, 2012

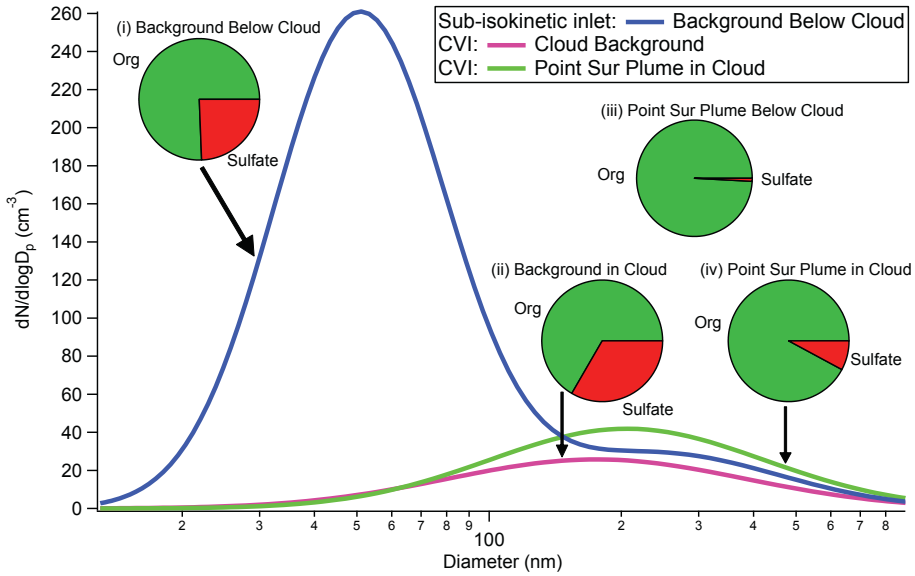

Fig. 9. DMA size distribution and AMS chemical composition measurements during Flight 6 from Figs. 7–8. The DMA data collected downstream of a sub-isokinetic inlet below cloud were fit to a two-term log-normal function while the size distributions downstream the CVI were fit to a single-term log-normal function. Only sulfate and non-refractory organics were observed above detection limits by the AMS, and their relative mass concentrations are depicted in the pie charts for four different conditions: (i)–(ii) background marine aerosol below cloud and in cloud behind the CVI; (iii)–(iv) *Point Sur* smoke below cloud and in cloud behind the CVI. DMA data are not available for the *Point Sur* smoke below cloud.

AMTD
5, 1515–1541, 2012